High Pressure Rheological Behavior of 1-Ethyl-3-methylimidazolium n-Hexylsulfate and Trihexyl(tetradecyl)phosphonium Tris(pentafluoroethyl)trifluorophosphate

Regueira, Teresa; Lugo, Luis; Comuñas, María J. P.; Fernández, Josefa

Published in:
Journal of Chemical and Engineering Data

Link to article, DOI:
10.1021/acs.jced.7b00181

Publication date:
2017

Document Version
Peer reviewed version

High pressure rheological behaviour of 1-ethyl-3-methylimidazolium n-hexylsulfate and trihexyl(tetradecyl)phosphonium tris(pentafluoroethyl)trifluorophosphate

Teresa Regueira[1,2], Luis Lugo[3], María J.P. Comuñas[1], Josefa Fernández[1,*]

[1]*Laboratorio de Propiedades Termofísicas, Grupo NaFoMat, Departamento de Física Aplicada, Universidade de Santiago de Compostela, 15782 Santiago de Compostela, Spain*
[2]*Center for Energy Resources Engineering (CERE), Department of Chemistry, Technical University of Denmark, DK-2800 Kgs. Lyngby, Denmark*
[3]*Departamento de Física Aplicada, Facultade de Ciencias, Universidade de Vigo, E-36310 Vigo, Spain*

*Corresponding author. Tel.: +34 881814046; fax: +34 881814112

E-mail address: josefa.fernandez@usc.es (J. Fernández).

Abstract

Ionic liquids have been broadly studied in the last decade for being used as lubricants or lubricant additives. The rheological characterization of these fluids is very important in this context because it determines to a great extent their performance for different lubricants applications, such as hydraulic or gear lubricants. Thus, in this work we have performed the rheometric characterization of two ionic liquids (ILs), 1-ethyl-3-methylimidazolium n-hexylsulfate and trihexyl(tetradecyl)phosphonium tris(pentafluoroethyl)trifluorophosphate, in the temperature range from 298.15 K to 353.15 K up to 75 MPa and shear rates up to 1000 s^{-1}. For this aim, the setup of a new device for rheological characterization at high pressure based on Couette flow and concentric cylinders was undertaken in this work. Moreover the pressure-viscosity and temperature-viscosity coefficients of these ILs have been calculated. Both ILs present Newtonian behaviour in the studied conditions. The trifluorophosphate IL has strong pressure-viscosity dependence whereas for the other IL this dependence is quite slight.

Keywords: Rheology; High pressure; Ionic liquid; Lubricant; Viscosity.

1. INTRODUCTION

Nowadays high pressure rheology is gaining growing interest in several areas such as the crude oil extraction, polymers high-pressure treatment and processing of foods, basic research in chemistry, physics and geophysics, fuels for diesel engines, high-pressure extraction processes using supercritical fluids, high-pressure impregnation and coating, innovative solvent technology based on ionic liquids and semiconductor and nanoparticle industries.[1] Among many applications, high pressure rheology is an important issue in the field of lubrication in order to characterize lubricants behaviour when subjected to high pressures.[1] This field comprises an important area because this technique allows the determination of the pressure-temperature-viscosity relationship[2]. Thus, in elastohydrodynamic lubrication (EHL), one of the main parameters governing the global contact behaviour is the fluid film thickness, which separates the solids under contact, and is controlled to a great extent by the lubricant high pressure rheology. It is important to mention that the lubricant film thickness is the main parameter studied in EHL contacts[3]. The classic formulas for the calculation of the film thickness require the knowledge of the pressure-viscosity coefficient, which can be determined from measurements of the low shear viscosity as a function of pressure up to moderate pressures. Non-Newtonian effects should be taken into account to evaluate the lubricant behaviour in the high-pressure EHL contacts.[4] Additionally, other interesting parameter to be considered in a EHL analysis is the temperature-viscosity coefficient[4].

High pressure rheometers can be classified into three groups, capillary, rotational (cone and plate, parallel plate and concentric cylinder geometries) and sliding plate rheometers. The advantages of rotational rheometers are: the viscosity measurements are made under steady-state conditions, there is negligible variation of shear rate and shear stress throughout the sample and they allow the study and characterization of Non-

Newtonian behaviour.[5, 6] However, rotational rheometers present some disadvantages, such as shear-induced dissipative conversion of mechanical energy into thermal energy, secondary flow caused by inertial forces (so-called Taylor vortices), slip on the shear surfaces, separation effects in suspensions and end effects.[1]

Literature on high pressure rheometry is scarce even though several authors have worked on this topic.[1, 4]. The earliest pressurized Couette viscometer appears to have been constructed by Thomas et al.[7], who placed an electric motor within the pressure vessel to drive the rotation. They experienced many problems with this arrangement and the heat generated by the motor was significant. Hutton and Phillips[8] overcame the problem of driving the rotation by passing a shaft through a high-pressure seal and situating the motor outside of the pressure vessel.[4] Hamilton and Bottomley[9] characterised the high pressure rheology behaviour of polymer-oil blends up to stresses of $5 \cdot 10^{-4}$ Pa through a high pressure Couette rheometer . Bair and Winer[10] developed a rotational Couette high-pressure, high-shear stress viscometer with a pressure capability of 300 MPa. Subsequently, Bair[4] built a similar rheometer that can be used up to 1 GPa. Briscoe et al.[11] have measured rheological properties by a modified Haake Searle-type viscometer, which was incorporated into a high temperature and pressure chamber, with a maximum operating pressure of 100 MPa. Khandare et al.[6, 12] have designed and developed a high-temperature, high-pressure rheometer to measure viscosity of pitch material at elevated temperatures. Larsson et al.[13] and Petterson[14, 15] have determined the pressure–viscosity relationship of lubricants by means of a Couette rheometer whose pressure can be raised to 500 MPa. Parris et al.[16] performed high pressure steady-shear rheological measurements in a Couette rheometer designed for pressures up to 238 MPa. Hwang et al.[17] determined rheological properties by means of a rotational viscometer adapted to measure the viscosity of polymer under high temperature and pressure

conditions. Martínez-Boza and his collaborators [18-20] has performed rheological studies on used motor oil/vacuum residue blends, bitumens, heavy oils, invert-emulsion oil muds, and drilling fluids with two controlled stress rheometers, RheoStress RS600 from Haake Gbr and MARS II, from Thermo Scientific using coaxial cylinder and double helical ribbon geometries. Sun et al. characterized a water/crude oil emulsion in the presence of methane with an Anton Paar (Graz, Austria) MCR302 rheometer, which temperature can be controlled between 123.15 K and 1273.15 K and up to 15 MPa.[21] Finally, modified Couette geometries have been recently proposed by Pandey et al.[22] to characterize forming gas hydrates. In this work we have undertaken the setup of a new device for rheological characterization at high pressure. The heart of the setup is a Reologica StressTech Couette HTHP rheometer equipped with a high pressure cell that allows measurements up to 100 MPa.

On the other hand, study of ionic liquids (ILs) as potential lubricants has greatly increased during the last decade, due to their main properties such as low volatility, high thermal stability and conductivity, low melting point, broad liquid range and low temperature fluidity[23-29]. There are several works that study the viscous behavior at constant shear rate with falling body viscometers[30-32], rotational viscometers[33-37], rolling ball viscometers[38], capillary viscometers[39] and vibrating wire viscometers[40], among others. Concerning rheological studies at not constant shear rates, there are only some publications at atmospheric pressure. Thus, Burrell et al.[41] studied the shear thinning of 14 protic and aprotic ionic liquids (ILs) by stress-controlled rheometry from 293 K from 353 K with shear rates from 10 to 8000 s^{-1} finding that only five ILs present Newtonian behaviour. Voeltz et al. Smith et al.[42] have found that some primary ammonium ILs behave as Newtonian fluids at low shear rates but shear thin at high shear. Camargo et al.[43] have found similar behaviour for five esters of hydroxylalkylammonium. Tao and

Simon[44] have found Non-Newtonian behaviour of a series of imidazolium-based ILs with cyclic and aromatic groups at low temperatures (from 215 to 241 K.).

In this work we have studied two ILs, 1-ethyl-3-methylimidazolium n-hexylsulfate and trihexyl(tetradecyl)phosphonium tris(pentafluoroethyl) trifluorophosphate, which have kinematic viscosities at 313.15 K and 0.1 MPa slightly higher than the values corresponding to ISOVG100 viscosity grade[45], as potential gear lubricants. We have performed rheological measurements of these two ILs up to 75 MPa and shear rates up to 1000 s^{-1}. Moreover, we have calculated the local and universal pressure-viscosity coefficient, as well as the temperature-viscosity coefficient, comparing the obtained results with those of some reference lubricants.

2. EXPERIMENTAL SECTION

2.1. Materials. Samples of 1-ethyl-3-methylimidazolium n-hexylsulfate, $[C_2C_1Im][C_6SO_4]$, and trihexyl(tetradecyl)phosphonium tris(pentafluoroethyl) trifluorophosphate, $[P_{6,6,6,14}][(C_2F_5)_3PF_3]$ were kindly provided by Merck KGaA. Prior to their use, samples were degassed under vacuum and agitation at least during 48 h. The water content was after measured through a Karl Fischer method using a Mettler Toledo DL32 coulometric titrator. Purity of the IL samples as well as the water content are presented in table 1.

2.2. Measurement Technique. In this work we have undertaken the setup of a new device for rheological characterization at high pressure. Reologica StressTech Couette HTHP rheometer is the core of the setup. As can be seen in Figure 1 this rheometer consists of a CC25 DIN53019 concentric cylinder geometry and relies on Couette flow, involving confinement of the sample between a stationary cup (inner cylinder) and a rotating bob (outer cylinder), with a 1 mm gap. The inner cylinder has a diameter of 25

mm and a length of 37.67 mm. The surfaces of bob and cup cylinders are smooth according to the information provided by the developers of this rheometer. The high pressure cell is equipped with inlet and outlet ports for sample loading. The cell is suitable for self-purging and does not have to be opened after each measurement. The structure of the instrument is composed by a motor module, in which the drag cup motor applies a torque to the rotor and the position sensor measures the angular deflection during rotation. As regards the motor, it is an AC asynchronous one, extremely linear from low to high torque with a smooth and continuous response around 360 degrees. The rotor is light, high strength aluminium alloy, and has low inertia allowing fast transient and high frequency response. Concerning motor temperature, it is maintained constant by using an external heat exchanger (motor cooler). This allows the rheometer to run at full power continuously without any change in motor temperature and thus change in torque output. To be able to close the cell completely from the environment, the torque is applied using a magnetic coupling. The whole system is running in a maintenance free air bearing to avoid friction between rotating and static parts. This type of bearing requires a clean supply of dry oil-free air of 5 l/min and ensures frictionless measurements. Clean and dry air is supported to the rheometer bearing by using an additional compressed air line with four SMC air filters (AMG 150C, AW20, AFM20 and AFD20). Figure 2 shows the rheometer setup.

The apparatus can perform controlled stress and controlled rate measurements. The rheometer can operate in a torque range between $1 \cdot 10^{-4}$ and $4 \cdot 10^{-2}$ N·m, which entails a maximum shear stress around 350 Pa. It can operate in a temperature range from ambient temperature to 493.15 K. The cell can be heated or cooled at programmed rates. The temperature control is performed through a Joule/Thomson approach, utilizing a single temperature control system (control box). In addition, a separate water circulator

(Huber CC505) is required to act as the cold side heat sink for the thermoelectric device. The temperature control system consists also of a thermocouple sensor and an electronic box. The thermocouple reading was corrected from 288.15 K to 363.15 K through a calibrated Pt-100 probe inserted inside the rheometer cup. The final expanded uncertainty (k=2) of the temperature readings is estimated to be ±0.5 K. Concerning pressure the rheometer cell can operate at pressures up to 100 MPa. The pressure in the cell is increased externally through a high pressure line consisting of a piston screw pump HiP model 50-6-15, a pressure transducer Digibar II K-PE-300 calibrated with an expanded uncertainty (k=2) of ±0.02 MPa, as well as high pressure tubes and valves connected to the ports of the measurement cell. This rheometer works along with the RheoExplorer software, thus a computer is used as the interface to allow the user to control the instrument, collect and analyze the resulting data.

2.3. Experimental procedure. To avoid contamination of the samples a syringe coupled to a Hamilton valve was connected to one of the ports of the high pressure rheometer cell (connected to V6 as can be seen in Figure 2), for sample loading. Prior to the loading of the samples by means of this Hamilton valve all the system is evacuated using a rotary vacuum pump Edwards RV3 connected to V7. Once the system is loaded V6 is closed. The temperature set point for the measurements is selected in the RheoExplorer software and the thermostatic bath temperature is automatically fixed at 5 K lower. Once the temperature is stable, the magnetic coupling gap of the rheometer is fixed to zero. The first tests that are performed to the sample are stress-time tests in order to know the minimum and maximum stress limits which give right results for our sample. Afterwards the flow curves at atmospheric pressure under controlled stress tests are performed in an automated way following the stress ramp imposed to the software. A delay time of 10 s and an integration time of 20 s for each measurement are usually selected. When

finished, pressure is increased by means of the piston screw pump and the measurement procedure is repeated. As soon as all the desired pressures are measured, the temperature set point is changed and the next isotherm measurements are carried out. Finally all the system must be cleaned with suitable solvents.

2.4. Calibration and uncertainty. In a typical Couette rheometer, the velocity or displacement of the moving surface and the force on one of the surfaces are the variables measured. By using mathematical relationships it is possible to relate the torque (M) with the shear stress (σ) and the angular velocity (Ω) with the shear rate ($\dot{\gamma}$), respectively[46]. In the literature there are previous publications[47-50] reporting the equations necessary to describe the rotational rheometers. Steffe[48] in a publication on rheological methods in food process engineering cite some of the assumptions made in developing the mathematical expression describing instrument. These assumptions[48] are: flow is laminar and steady, end effects are negligible, test fluid is incompressible, there is no slip at the walls of the instruments, and radial and axial velocity components are zero. As these authors[48-50] suggest the stress (σ) can be easily related with the torque trough the following expression:

$$\sigma = \frac{F}{A} = \frac{M/r}{A} = \frac{M/r}{2\pi Lr} = \frac{M}{2\pi Lr^2} \qquad (1)$$

where *r* is the radius, *L* is the length of the cell, *F* is the force, *M* is the torque and *A* the area. In this equation the relation between the force, the torque *M* and the radius r is also used. To find the relation between the angular velocity (Ω) with the shear rate ($\dot{\gamma}$) is it necessary to make some calculations. Thus, usually[48, 50] to calculate the shear rate ($\dot{\gamma}$) it is assumed that the fluid elements move in circles about the common axis of the cylinders with an angular velocity (ω) which is a function of radius (*r*) from the center to the position in the gap. Moreover the shear rate is a function of the stress. Thus, if we

study Newtonian fluids or power law fluids, the following relations (equation 2 and 3) will be respectively accomplished:

$$\dot{\gamma} = f(\sigma) = \frac{\sigma}{\eta} \tag{2}$$

$$\dot{\gamma} = f(\sigma) = \left(\frac{\sigma}{K}\right)^{1/n} \tag{3}$$

So, in general we can write:

$$\dot{\gamma} = -r\frac{d\omega}{dr} = f(\sigma) \tag{4}$$

It is possible to express dr as a function of dσ by differentiating equation (1), that is:

$$\frac{dr}{d\sigma} = \sqrt{\frac{2\pi L r^2 \sigma}{2\pi L}} \left(\frac{-1}{2}\right) \sigma^{-3/2} = \frac{-r}{2\sigma} \tag{5}$$

From the combination of equations (4) and (5) it can be obtained the relation between the angular velocity of the bob and the shear stress in the gap:

$$\Omega = -\frac{1}{2}\int_{\sigma_1}^{\sigma_2} \mathrm{f}(\sigma)\frac{\mathrm{d}\sigma}{\sigma} \tag{6}$$

Being 1 the inner cylinder and 2 the outer cylinder. In the rheometer used in this work the inner cylinder is the moving surface ($\omega=\Omega$) and the outer cylinder the stationary surface ($\omega=0$). For Newtonian fluids equation (2) is accomplished and consequently:

$$\Omega = -\frac{1}{2}\int_{\sigma_1}^{\sigma_2}\frac{\sigma}{\eta}\frac{d\sigma}{\sigma} = \frac{1}{2\eta}\left(\sigma_1 - \sigma_2\right) \tag{7}$$

Using equation (1) to calculate the stress in the inner (r=R1) and in the outer (r=R2) cylinder allows writing equation (7) as:

$$\Omega = \frac{M}{4\pi L\eta}\left(\frac{1}{R_1^2} - \frac{1}{R_2^2}\right) \tag{8}$$

This expression is called Margules equation and describes the behaviour of a Newtonian fluid in a concentric rheometer. From equation (2) by the substitution of the value of σ obtained from equation (1), as well as the value of η given by the Margules yields:

$$\dot{\gamma} = \frac{2}{r^2}\left(\frac{1}{R_1^2} - \frac{1}{R_2^2}\right)^{-1} \Omega \tag{9}$$

In a typical Couette rheometer, velocity or displacement of the moving surface and the force on one of the surfaces are the variables measured. By using equation (1) and (9) it is possible to relate the torque with the shear stress and the angular velocity with the shear rate, respectively. Both equations can be rewritten as follows:

$$\sigma = C_\sigma \cdot M \tag{10}$$

$$\dot{\gamma} = C_\gamma \cdot \Omega \tag{11}$$

where C_σ and C_γ are geometrical constants defined according to the following equations:

$$C_\sigma = \frac{1}{2\pi r^2 L} \tag{12}$$

$$C_\gamma = \frac{2}{r^2}\left(\frac{1}{R_1^2} - \frac{1}{R_2^2}\right)^{-1} \tag{13}$$

So, theoretically by using the geometrical constants (equations 12 and 13) it should be possible to obtain the stress from the torque and the shear rate from the angular velocity. Subsequently, the dynamic viscosity could be determined. Notice here that equations (10 to 13) have been derived considering valid equation (2), that is assuming that the fluid in Newtonian. In practice, the use of these equations is not sufficient to determine accurately dynamic viscosity or flow curves. Not only due to the assumption that the fluid has a linear relation between $\dot{\gamma}$ and σ through the viscosity, but also due to other aspects that should be considered for concentric cylinder rheometers. One of them is the

inertia of rotor, thus the stress necessary to overcome the inertia of rotor and measurement system, can be a substantial part of the applied stress. This aspect is more significant for measurements on low viscous samples. Another aspect is the friction. The Reologica HTHP rheometer used in this work is running in an air bearing to reduce friction between rotating and static parts. The friction in the bearing of the rotating part should be very low where the angular deflection is detected because it would decrease the rotational speed and the calculated viscosity values would be higher than the real value. As Steffe[48] remarks, another important fact is the end-effects that can influence rheological measurements, thus it is important to account for the influence of the bottom of the cylinder on the torque response of the system. Schramm[49] suggests also that it is necessary to control the wall effects. They occur when the adherence between the moving surface and the liquid is insufficient to transmit the shear stress and the surface slips above the non-moving liquid sample.

In this work, in a first moment we have tried to use the values of C_σ and C_γ reported in the technical specifications of the Reologica HTHP rheometer and included in the RheoExplorer software. With the values of these geometrical constants we have tried to reproduce the dynamic viscosity values of two Newtonian fluids, squalane (SQN) and diisodecyl phthalate (DIDP). The dynamic viscosity of both these fluids is accurately reported in literature[51-55] over wide temperature and pressure intervals. We have observed that the dynamic viscosity obtained with Reologica HTHP rheometer finding higher that the reference values of SQN and DIDP. Subsequently, we have selected more viscous fluids (polyalphaolefin, PAO40 and polybutene, H8) with the aim to reduce the effect of the inertia of the motor. Moreover we have decided to calibrate the rheometer for each sample and temperature using for that the viscosity values at atmospheric pressure measured in a high precision rotational SVM 3000 Stabinger viscometer. The correction

of viscosity values performed at atmospheric pressure is assumed to be the same overall the pressure range. In this sense we should remark that they are scarce publications in the literature giving precise details on calibration method used for rotational rheometers, even less for rheometer working at high pressures. Finally, as the uncertainty of this rheometric technique is not established in the equipment specifications, it was analyzed in this work by comparison of the results obtained for polyalphaolefin (PAO40) and polybutene (H8) with those of the literature.

3. RESULTS

Firstly, the accuracy determination of high pressure viscosity has been checked studying PAO40[56] and also of polybutene H8[57] in Newtonian conditions. For the PAO 40, an percentage absolute average deviation, AAD%, of 7% in the temperature range from 298.15 K to 353.15 K up to 75 MPa with correlated data from Bair[58] was obtained. Also, for the polybutene H8, viscosity values were also compared with correlated data from Bair[58, 59] obtaining an AAD% around 10%. The relative deviations we have found for PAO 40 and polybutene H8 are plotted in Figure 3. Taking into account the uncertainty of the rheometer used by Bair[58] we estimate that the expanded uncertainty (k=2) of our equipment is 7%.

Subsequently, rheological flow tests were performed up to shear rates of 1000 s^{-1} for both ILs at temperatures between 298.15 K and 353.15 K up to 75 MPa. As example, a flow test is presented in Figure 4 for both ILs at 298.15 K for the different pressures. A Newtonian behaviour was found for the studied ILs in the temperature, pressure and shear rate ranges analysed in this work. The reference viscosity values at atmospheric pressure employed for calibration were taken from Gaciño et al.[37] and the obtained viscosity values at high pressure are presented in Table 2. The viscosity values of

$[P_{6,6,6,14}][(C_2F_5)_3PF_3]$ are higher than those of $[C_2C_1Im][C_6SO_4]$. These viscosity values were correlated as a function of temperature and pressure by means of the following Comuñas et al.[60] correlation, for which those viscosity data at atmospheric pressure from Gaciño et al.[37] were also employed:

$$\eta(p,T)=A\left(\frac{p+E_0+E_1T+E_2T^2}{p_{ref}+E_0+E_1T+E_2T^2}\right)^D \exp\left(\frac{B}{T-C}\right) \quad (14)$$

Coefficients of this adjustment are presented in Table 3. The parameters *A*, *B* and *C* were obtained from the correlation of previously reported viscosity values[37] at ambient pressure as a function of temperature. Moreover, correlated values are plotted along with the experimental ones as a function of temperature for the different pressures in Figure 5. It can be observed that the influence of pressure on viscosity is stronger for $[P_{6,6,6,14}][(C_2F_5)_3PF_3]$. This in agreement with results obtained previously in our laboratory with other three ILs based on $[(C_2F_5)_3PF_3]^-$ anion: one based in a trialkylimidazolium cation[61, 62] $[C_4C_1C_1Im][(C_2F_5)_3PF_3]$, another on 1-butyl-1-methylpyrrolidinium[30] $[C_4C_1Pyrr][(C_2F_5)_3PF_3]$ and the other contains the 1-(2-methoxyethyl)1-methyl-pyrrolidinium cation[45, 46] $[C_1OC_2C_1Pyrr][(C_2F_5)_3PF_3]$.

We have performed a comparison between the viscosity values obtained for $[C_2C_1Im][C_6SO_4]$ and $[P_{6,6,6,14}][(C_2F_5)_3PF_3]$ and some data previously published[63] for four gear lubricants with the same an viscosity grade (ISOVG100). The gear lubricants are a mineral oil, a biodegradable synthetic ester, a polyalphaolefin and a polyalkylene glycol. In average, viscosity values of $[C_2C_1Im][C_6SO_4]$ and $[P_{6,6,6,14}][(C_2F_5)_3PF_3]$ are 19% and 46% higher than these gear lubricants[63], respectively. This comparison is depicted as a function of temperature at 50 MPa in Figure 6. It is important to note that our experimental viscosity values for $[C_2C_1Im][C_6SO_4]$ are very close to those for the

polyalkylene glycol[63], AAD% in the whole experimental temperature and pressure range is 11%, whereas the maximum difference is 30%.

The local pressure-viscosity coefficient, α, is employed for the characterization the viscosity pressure dependence of lubricants and it is defined by means of the following equation:

$$\alpha(p) = \frac{1}{\eta}\left(\frac{\partial \eta}{\partial p}\right)_T \tag{15}$$

This coefficient is frequently used to quantify the EHL film-generating capability of a lubricant[64]. We have calculated this property by differentiation from the $\eta(T,p)$ correlation and it is plotted in Figure 7 for the two studied ILs . It can be observed that $\alpha(p)$ diminishes both with temperature and pressure and that $[P_{6,6,6,14}][(C_2F_5)_3PF_3]$ has higher values of this property than $[C_2C_1Im][C_6SO_4]$. Gaciño et al.[30, 61] have previously found that other ILs with the anion $[(C_2F_5)_3PF_3]^-$ present also higher local pressure viscosity coefficients than those with the anions bis(trifluoromethylsulfonyl)imide $[NTf_2]^-$ and trifluoromethanesulfonate $[CF_3SO_3]^-$.

Additionally, we have performed in Figure 8 a comparison between the local pressure-viscosity coefficient of the ILs studied in this work with other fluids from literature at 313.15 K, i.e. an IL based on $[(C_2F_5)_3PF_3]^-$ anion, a polyalkylene glycol (PAG3)[65], squalane[52] as well as the mineral oil, the biodegradable synthetic ester, the polyalphaolefin 0 and the polyalkyleneglycol measured by Gold et al.[63]. It can be observed that the highest local pressure-viscosity coefficients are obtained for squalane, the four $[(C_2F_5)_3PF_3]^-$ ILs and PAG3 whereas the lowest values are obtained for both alkyl sulfate ILs. It also can be seen that the effect of the increasing four methylene groups in the imidazolium cation increases quite strongly the local pressure-viscosity coefficient.

Another interesting parameter for characterizing fluids for lubricant applications is the universal pressure-viscosity coefficient, $\alpha_{film,}$ which is independent of pressure and it is given by the following equation[66]:

$$\alpha_{film} = \frac{1-\exp(-3)}{p_{iv}(3/\alpha^{*})} \tag{16}$$

where p_{iv} (isoviscous pressure) and α^{*} (piezo-viscous coefficient) are defined as follows:

$$p_{iv}(p) = \int_{0}^{p} \frac{\eta(p'=0)dp'}{\eta(p')} \tag{17}$$

$$\alpha^{*} = \frac{1}{p_{iv}(\infty)} = \left[\int_{0}^{\infty} \frac{\eta(p=0)dp}{\eta(p)}\right]^{-1} \tag{18}$$

The universal pressure-viscosity coefficients were calculated for the ILs studied in this work and are reported in Table 4 and for the different temperatures. It is observed that the α_{film} values of $[P_{6,6,6,14}][(C_2F_5)_3PF_3]$ are near the double of those of $[C_2C_1Im][C_6SO_4]$. The values obtained for the first IL are similar to those of $[C_4C_1Pyrr][(C_2F_5)_3PF_3]$ and $[C_4C_1Pyrr][(C_2F_5)_3PF_3]$ and quite bigger than those of several ILs based of $[NTf_2]^-$, $[CF_3SO_3]^-$. tetraborofluorate ($[BF_4]^-$), hexafluorophosphate ($[PF_6]^-$), tosylate ($[TOS]^-$ and alkyl sulfate ($[C_2SO_4]^-$, $[C_1SO_4]^-$) anions[30, 62, 65, 67].

The pressure-viscosity coefficients are needed to determine the central film thickness (h_c) of the lubricants in rolling elements under EHL conditions. Several definitions of the pressure-viscosity coefficients[66] were used for this aim: the local pressure-viscosity coefficient at different pressure conditions (0.1 MPa or another pressure) or the piezo-viscous coefficient highest, among others. Bair et al.[66] and Liu et al.[68] showed that the definition of α_{film} given by equation (16) provide values for the central thickness, which are coherent with those obtained from interferometry experiments.

In order to analyze the effect of the lubricant in the central thickness (h_c), we have used the following equation[64] proposed by the American Gear Manufactures Association (AGMA) for calculation of h_c:

$$h_c = k\eta_0^{0.69}\alpha^{0.56}U^{0.69} \quad (19)$$

where η_0 is the viscosity at atmospheric pressure, U the relative speed of the rolling element and k is a parameter that depends on surface geometry, the applied load and the elastic parameters of the rolling elements. For the viscosity pressure coefficient, α, needed in equation (19), we have chosen, as in previous articles[30, 62, 65, 67, 69], the definition of α_{film} given by equation (16). If geometry, elastic properties, speed and loads are fixed, EHL film central thickness varies with two properties of the lubricant: the universal pressure-viscosity coefficient and the absolute viscosity, as follows[64]:

$$h_c \propto \eta_0^{0.69}\alpha_{film}^{0.56} \quad (20)$$

Thus, we have plotted in Figure 9 $\eta_0^{0.69}\alpha_{film}^{0.56}$ against temperature for the studied ILs, finding that under the same EHL conditions, $[P_{6,6,6,14}][(C_2F_5)_3PF_3]$ would have a thicker central thickness than $[C_2C_1Im][C_6SO_4]$. In previous papers[30, 62, 65, 67, 69] we have evaluated the factor due to the lubricant $\eta_0^{0.69}\alpha_{film}^{0.56}$ for 19 ILs and 13 mineral, synthetic or vegetable oils. Only the IL $[C_8C_1Im][PF_6]$, whose kinematic viscosity at 313 K is 226 mm^2s^{-1}, present higher values that those obtained for $[P_{6,6,6,14}][(C_2F_5)_3PF_3]$. As $[PF_6]^-$ based ILs present corrosion problems due to their reactivity, when a thick $[P_{6,6,6,14}][(C_2F_5)_3PF_3]$ to protect the surfaces against wear is required $[P_{6,6,6,14}][(C_2F_5)_3PF_3]$ seems to be a good option as lubricant for rolling elements.

Finally, we have calculated the temperature-viscosity coefficient, β, which is given by the following equation:

$$\beta = -\frac{1}{\eta}\left(\frac{\partial \eta}{\partial T}\right)_p \tag{21}$$

The obtained values of the temperature-viscosity coefficient are presented in Figure 10. This property depends highly on temperature, decreasing with the temperature increase, whereas the dependence on pressure is rather smooth. It has be found that the values of this property are very similar for both ILs, 4% being the difference. In figures 10 (a and b) the β values of $[C_4C_1Pyrr][(C_2F_5)_3PF_3]$ and $[C_4C_1Pyrr][CF_3SO_3]$ were also included. The lowest β values, i.e. lowest viscosity-temperature dependence, of the last IL are in agreement with the fact that its viscosity index (VI=156) is higher than those of the other three ILs $[C_2C_1Im][C_6SO_4]$, $[P_{6,6,6,14}][(C_2F_5)_3PF_3]$ and $[C_4C_1Pyrr][(C_2F_5)_3PF_3]$ whose VI is respectively 136, 128, 119.

4. CONCLUSIONS

The rheological characterization of $[C_2C_1Im][C_6SO_4]$ and $[P_{6,6,6,14}][(C_2F_5)_3PF_3]$ was performed in this work from 298.15 K to 353.15 K, up to 75 MPa and shear rates up to $1000s^{-1}$. It was found a Newtonian behaviour for both ILs under the studied conditions, finding viscosity values higher for $[P_{6,6,6,14}][(C_2F_5)_3PF_3]$ than for $[C_2C_1Im][C_6SO_4]$. Moreover, these viscosity values were compared with those of different reference oils for gear applications, finding that viscosity values of $[C_2C_1Im][C_6SO_4]$ are close to those of a polyalkylene glycol with ISO VG of 100. Additionally we have calculated the viscosity derived properties $\alpha(p)$ and β. For the first of them, it was observed that values for $[P_{6,6,6,14}][(C_2F_5)_3PF_3]$ are of the same order than literature values for squalane[52] and also higher than those for $[C_2C_1Im][C_6SO_4]$. As regard the temperature-viscosity coefficient, very similar values (around 4%) were found for the studied ILs. Finally, α_{film} values of $[P_{6,6,6,14}][(C_2F_5)_3PF_3]$ were found to be near double than those of $[C_2C_1Im][C_6SO_4]$.

Funding

This work was supported by Spanish Ministry of Economy and Competitiveness and the UE FEDER programme through CTQ2011-23925, ENE2014-55489-C2-1-R and ENE2014-55489-C2-2-R projects as well as by Xunta de Galicia through the EM2013/031 and GRC ED431C 2016/001 programmes and the Galician Network on Ionic Liquids ReGaLIs R2014/015.

ACKNOWLEDGEMENTS

We express our gratitude to Prof. Martínez-Boza (University of Huelva, Spain) for his useful advice. Authors acknowledge the samples provided by Merck KGaA (Ionic Liquids), Ineos Oligomers (Polybutene) and REPSOL (PAO40).

This paper was part of the Doctoral Thesis of T. Regueira.[70]

References

1. Kulisiewicz, L.; Delgado, A. High-pressure rheological measurement methods: A review. *App. Rheol.* **2010,** 20, 13018-1-15.
2. Boza, F. J. M.; Gallegos, C. High pressure rheology. In *Rheology*, Gallegos, C.; Walters, K., Eds. Encyclopedia of chemical sciences, engineering and technology resources (Encyclopedia of life support systems): 2009; Vol. I.
3. Berthe, D.; Vergne, P. High pressure rheology for high pressure lubrication: A review. *J. Rheol.* **1990,** 34, 1387-1414.
4. Bair, S. S. *High-pressure rheology for quantitative elastohydrodynamics* 1st ed.; Elsevier: Amsterdam, 2007.
5. Garratt, G. W.; Rand, B.; Whitehouse, S. An apparatus for studying the rheological behaviour of carbonaceous materials at elevated temperature and pressure. *Fuel* **1988,** 67, 238-241.
6. Khandare, P. M.; Zondlo, J. W.; Stansberry, P. B.; Stiller, A. H. Rheological investigation of pitch materials: Part I: Design and development of a high-temperature high-pressure (HTHP) rheometer. *Carbon* **2000,** 38, 881-887.
7. Thomas, B. W.; Ham, W. R.; Dow, R. B. Viscosity-pressure characteristics of lubricating oils. *Ind. Eng. Chem.* **1939,** 31, 1267-1270.
8. Hutton, J.; Phillips, M. High pressure viscosity of a polyphenyl ether measured with a new Couette viscometer. *Nature* **1973,** 245, 15-16.
9. Hamilton, G. M.; Bottomley, L. Measurement of viscosity loss of polymer-containing oils at high shear stresses. *Trib. Int.* **1987,** 20, 41-48.
10. Bair, S.; Winer, W. O. A new high-pressure, high-shear stress viscometer and results for lubricants. *Tribol. Trans.* **1993,** 36, 721-725.
11. Briscoe, B.; Luckham, P.; Zhu, S. Rheological study of poly(ethylene oxide) in aqueous salt solutions at high temperature and pressure. *Macromolecules* **1996,** 29, 6208-6211.
12. Khandare, P. M.; Zondlo, J. W.; Stansberry, P. B.; Stiller, A. H. Rheological investigations of pitch material: Part II: viscosity measurement of A240 and ARA-24 pitches using a high-temperature high-pressure rheometer. *Carbon* **2000,** 38, 889-897.
13. Larsson, R.; Larsson, P. O.; Eriksson, E.; Sjöberg, M.; Höglund, E. Lubricant properties for input to hydrodynamic and elastohydrodynamic lubrication analyses. *Proc. Inst. Mech. Eng., Part J* **2000,** 214, 17-27.
14. Pettersson, A. Tribological characterization of environmentally adapted ester based fluids. *Trib. Int.* **2003,** 36, 815-820.
15. Pettersson, A. High-performance base fluids for environmentally adapted lubricants. *Trib. Int.* **2007,** 40, 638-645.
16. Parris, M. D.; MacKay, B. A.; Rathke, J. W.; Klingler, R. J.; Gerald, R. E. Influence of pressure on boron cross-linked polymer gels. *Macromolecules* **2008,** 41, 8181-8186.
17. Hwang, T.; Kim, M.; Ahn, Y.; Lee, J. In *The high pressure rheology of polymer nanocomposites containing supercritical carbon dioxide*, 68th Annual technical conference of the society of plastics engineers (ANTEC 2010), Orlando, Florida, 2010; Curran Associates, Inc.: Orlando, Florida, 2010; pp 1095-1098.
18. Martínez-Boza, F.; Fernández-Latorre, F.; Gallegos, C. High-pressure viscosity of used motor oil/vacuum residue blends. *Fuel* **2009,** 88, 1595-1601.
19. Hermoso, J.; Martinez-Boza, F.; Gallegos, C. Influence of viscosity modifier nature and concentration on the viscous flow behaviour of oil-based drilling fluids at high pressure. *Appl. Clay Sci.* **2014,** 87, 14-21.
20. Hermoso, J.; Martinez-Boza, F.; Gallegos, C. Influence of aqueous phase volume fraction, organoclay concentration and pressure on invert-emulsion oil muds rheology. *J. Ind. Eng. Chem.* **2015,** 22, 341-349.

21. Sun, L.; Yang, G.; Wang, Y.; Jing, D. Experimental study on high-pressure rheology of water/crude oil emulsion in the presence of methane. *J. Dispersion Sci. Technol.* **2017,** 38, 789-795.
22. Pandey, G.; Linga, P.; Sangwai, J. S. High pressure rheology of gas hydrate formed from multiphase systems using modified Couette rheometer. *Rev. Sci. Instrum.* **2017,** 88, 025102.
23. Libardi, A.; Schmid, S. R.; Sen, M.; Schneider, W. In *Evaluation of ionic fluids as lubricants in manufacturing*, Transactions of the North American Manufacturing Research Institution of SME, 2013; 2013; pp 121-127.
24. Tiago, G.; Restolho, J.; Forte, A.; Colaço, R.; Branco, L. C.; Saramago, B. Novel ionic liquids for interfacial and tribological applications. *Colloid Surf. A-Physicochem. Eng. Asp.* **2015,** 472, 1-8.
25. Li, Z.; Ren, T. Synergistic effects between alkylphosphate-ammonium ionic liquid and alkylphenylborate as lubricant additives in rapeseed oil. *Tribol. Int.* **2017,** 109, 373-381.
26. Hernández Battez, A.; Fernandes, C. M. C. G.; Martins, R. C.; Bartolomé, M.; González, R.; Seabra, J. H. O. Two phosphonium cation-based ionic liquids used as lubricant additive: Part I: Film thickness and friction characteristics. *Tribol. Int.* **2017,** 107, 233-239.
27. Plechkova, N. V.; Seddon, K. R. Applications of ionic liquids in the chemical industry. *Chem. Soc. Rev.* **2008,** 37, 123-150.
28. Freemantle, M. New frontiers for ionic liquids. *Chem. Eng. News* **2007,** 85, 23-26.
29. Zhao, H. Innovative applications of ionic liquids as 'green' engineering liquids. *Chem. Eng. Commun.* **2006,** 193, 1660 - 1677.
30. Gaciño, F. M.; Comuñas, M. J. P.; Regueira, T.; Segovia, J. J.; Fernández, J. On the viscosity of two 1-butyl-1-methylpyrrolidinium ionic liquids: Effect of the temperature and pressure. *J. Chem. Thermodyn.* **2015,** 87, 43-51.
31. Harris, K. R.; Woolf, L. A.; Kanakubo, M.; Rüther, T. Transport properties of n-butyl-n-methylpyrrolidinium bis(trifluoromethylsulfonyl)amide. *J. Chem. Eng. Data* **2011,** 56, 4672-4685.
32. Qiao, Y.; Yan, F.; Xia, S.; Ma, P. Densities and viscosities of 1-butyl-3-methylimidazolium hexafluorophosphate [bmim][PF6] + CO2 binary system: determination and correlation. *Chin. J. Chem. Eng.* **2013,** 21, 1284-1290.
33. Safarov, J.; Kul, I.; El-Awady, W. A.; Nocke, J.; Shahverdiyev, A.; Hassel, E. Thermophysical properties of 1-butyl-4-methylpyridinium tetrafluoroborate. *J. Chem. Thermodyn.* **2012,** 51, 82-87.
34. Lee, H.; Cho, M. H.; Lee, B. S.; Palgunadi, J.; Kim, H.; Kim, H. S. Alkyl-fluoroalkylimidazolium-Based Ionic Liquids as Efficient CO2 Absorbents. *Energy Fuels* **2010,** 24, 6689-6692.
35. Ferreira, C. E.; Talavera-Prieto, N. M. C.; Fonseca, I. M. A.; Portugal, A. T. G.; Ferreira, A. G. M. Measurements of pVT, viscosity, and surface tension of trihexyltetradecylphosphonium tris(pentafluoroethyl)trifluorophosphate ionic liquid and modelling with equations of state. *J. Chem. Thermodyn.* **2012,** 47, 183-196.
36. Costa, A. J. L.; Esperança, J. M. S. S.; Marrucho, I. M.; Rebelo, L. P. N. Densities and Viscosities of 1-Ethyl-3-methylimidazolium n-Alkyl Sulfates. *J. Chem. Eng. Data* **2011,** 56, 3433-3441.
37. Gaciño, F. M.; Regueira, T.; Lugo, L.; Comuñas, M. J. P.; Fernández, J. Influence of molecular structure on densities and viscosities of several ionic liquids. *J. Chem. Eng. Data* **2011,** 56, 4984-4999.
38. Stevanovic, S.; Costa Gomes, M. F. Solubility of carbon dioxide, nitrous oxide, ethane, and nitrogen in 1-butyl-1-methylpyrrolidinium and trihexyl(tetradecyl)phosphonium tris(pentafluoroethyl)trifluorophosphate (eFAP) ionic liquids. *J. Chem. Thermodyn.* **2013,** 59, 65-71.
39. Widegren, J. A.; Magee, J. W. Density, Viscosity, Speed of Sound, and Electrolytic Conductivity for the Ionic Liquid 1-Hexyl-3-methylimidazolium

Bis(trifluoromethylsulfonyl)imide and Its Mixtures with Water. *J. Chem. Eng. Data* **2007,** 52, 2331-2338.
40. Diogo, J. C. F.; Caetano, F. J. P.; Fareleira, J. M. N. A.; Wakeham, W. A. Viscosity measurements of three ionic liquids using the vibrating wire technique. *Fluid Phase Equilib.* **2013,** 353, 76-86.
41. Burrell, G. L.; Dunlop, N. F.; Separovic, F. Non-Newtonian viscous shear thinning in ionic liquids. *Soft Matter* **2010,** 6, 2080-2086.
42. Smith, J. A.; Webber, G. B.; Warr, G. G.; Atkin, R. Rheology of protic ionic liquids and their mixtures. *J. Phys. Chem. B.* **2013,** 117, 13930-13935.
43. Camargo, D.; Andrade, R. S.; Ferreira, G. A.; Mazzer, H.; Cardozo-Filho, L.; Iglesias, M. Investigation of the rheological properties of protic ionic liquids. *J. Phys. Org. Chem.* **2016,** 29, 604-612.
44. Tao, R.; Simon, S. L. Rheology of imidazolium-based ionic liquids with aromatic functionality. *J. Phys. Chem. B.* **2015,** 119, 11953-11959.
45. Regueira, T.; Lugo, L.; Fernández, J. Ionic liquids as hydraulic fluids: comparison with conventional oils. *Lubr. Sci.* **2014,** 26, 488-499.
46. Estellé, P.; Lanos, C.; Perrot, A. Processing the Couette viscometry data using a Bingham approximation in shear rate calculation. *J. Non-Newtonian Fluid Mech.* **2008,** 154, 31-38.
47. Macosko, C. W. *Rheology : principles, measurements and applications*. Wiley-VCH: New York, 1994.
48. Steffe, J. F. *Rheological methods in food process engineering*. 2nd ed.; Freeman Press: East Lansing, MI, 1996.
49. Schramm, G. *A practical approach to rheology and rheometry*. 2nd ed.; Thermo electron (Karlsruhe) GmbH: Karlsruhe, 2004.
50. Tadros, T. F. *Rheology of Dispersions Principles and Applications*. Wiley-VCH: Weinheim, Germany, 2010.
51. Comuñas, M. J. P.; Paredes, X.; Gaciño, F. M.; Fernández, J.; Bazile, J.-P.; Boned, C.; Daridon, J.-L.; Galliero, G.; Pauly, J.; Harris, K. R. Viscosity measurements for squalane at high pressures to 350 MPa from T = (293.15 to 363.15) K. *J. Chem. Thermodyn.* **2014,** 69, 201-208.
52. Mylona, S. K.; Assael, M. J.; Comuñas, M. J. P.; Paredes, X.; Gaciño, F. M.; Fernández, J.; Bazile, J. P.; Boned, C.; Daridon, J. L.; Galliero, G.; Pauly, J.; Harris, K. R. Reference Correlations for the Density and Viscosity of Squalane from 273 to 473 K at Pressures to 200 MPa. *J. Phys. Chem. Ref. Data* **2014,** 43, 013104.
53. Schmidt, K. A. G.; Pagnutti, D.; Curran, M. D.; Singh, A.; Trusler, J. P. M.; Maitland, G. C.; McBride-Wright, M. New Experimental Data and Reference Models for the Viscosity and Density of Squalane. *J. Chem. Eng. Data* **2015,** 60, 137-150.
54. Al Motari, M. M.; Kandil, M. E.; Marsh, K. N.; Goodwin, A. R. H. Density and Viscosity of Diisodecyl Phthalate C6H4(COOC10H21)2, with Nominal Viscosity at T = 298 K and p = 0.1 MPa of 87 mPa·s, at Temperatures from (298.15 to 423.15) K and Pressures up to 70 MPa. *J. Chem. Eng. Data* **2007,** 52, 1233-1239.
55. Paredes, X.; Fandiño, O.; Comuñas, M. J. P.; Pensado, A. S.; Fernández, J. Study of the effects of pressure on the viscosity and density of diisodecyl phthalate. *J. Chem. Thermodyn.* **2009,** 41, 1007-1015.
56. Regueira, T., Comuñas, M.J.P., Lugo, L., Paredes, X., and Fernández, J. Implementation of a concentric cylinder rheometer for high pressures In 19th European Conference on Thermophysical Properties, Thessaloniki, Greece.: 2011.
57. Regueira, T.; Lugo, L.; Comuñas, M. J. P.; Fernández, J. In *High pressure rheometric characterization of a polybutene*, Ibereo 2011 Rheology Trends: from Nano to Macro Systems, Caparica, Portugal, 7-9 September 2011; Caparica, Portugal, 7-9 September 2011; pp 313-316.
58. Bair, S. Pressure-viscosity behavior of lubricants to 1.4 GPa and its relation to EHD traction. *Tribol. Trans.* **2000,** 43, 91-99.

59. Bair, S. The high-pressure, high-shear stress rheology of a polybutene. *J. Non-Newtonian Fluid Mech.* **2001,** 97, 53-65.
60. Comuñas, M. J. P.; Baylaucq, A.; Boned, C.; Fernández, J. High-pressure measurements of the viscosity and density of two polyethers and two dialkyl carbonates. *Int. J. Thermophys.* **2001,** 22, 749-768.
61. Gaciño, F. M.; Paredes, X.; Comuñas, M. J. P.; Fernández, J. Pressure dependence on the viscosities of 1-butyl-2,3-dimethylimidazolium bis(trifluoromethylsulfonyl)imide and two tris(pentafluoroethyl)trifluorophosphate based ionic liquids: New measurements and modelling. *J. Chem. Thermodyn.* **2013,** 62, 162-169.
62. Fernández, J.; Paredes, X.; Gaciño, F. M.; Comuñas, M. J. P.; Pensado, A. S. Pressure-viscosity behaviour and film thickness in elastohydrodynamic regime of lubrication of ionic liquids and other base oils. *Lubr. Sci.* **2014,** 26, 449-462.
63. Gold, P. W.; Schmidt, A.; Dicke, H.; Loos, J.; Assmann, C. Viscosity–pressure–temperature behaviour of mineral and synthetic oils. *J. Synth. Lubr.* **2001,** 18, 51-79.
64. Errichello, R. Selecting Oils with High Pressure-Viscosity Coefficient - Increase Bearing Life by More Than Four Times. *Mach. Lubr.* **2004,** http://www.machinerylubrication.com/Read/586/viscosity-coefficient-bearing.
65. Paredes, X.; Fandino, O.; Pensado, A. S.; Comunas, M. J. P.; Fernandez, J. Pressure-viscosity coefficients for polyalkylene glycol oils and other ester or ionic lubricants. *Trib. Lett.* **2012,** 45, 89-100.
66. Bair, S.; Yuchuan, L.; Wang, Q. J. The pressure-viscosity coefficient for Newtonian EHL film thickness with general piezoviscous response. *J. Tribol.* **2006,** 128, 624-631.
67. Pensado, A. S.; Comuñas, M. J. P.; Fernández, J. The Pressure–Viscosity Coefficient of Several Ionic Liquids. *Tribol. Lett.* **2008,** 31, 107-118.
68. Liu, Y.; J. Wang, Q.; Wang, W.; Hu, Y.; Zhu, D.; Krupka, I.; Hartl, M. EHL simulation using the free-volume viscosity model. *Tribol. Lett.* **2006,** 23, 27-37.
69. Paredes, X.; Comuñas, M. J. P.; Pensado, A. S.; Bazile, J.-P.; Boned, C.; Fernández, J. High pressure viscosity characterization of four vegetable and mineral hydraulic oils. *Ind. Crops. Prod.* **2014,** 54, 281-290.
70. Regueira, T. High pressure thermophysical behaviour of reference and new lubricants. Mineral, synthetic and vegetable oils and ionic liquids, PhD Thesis. PhD, University of Santiago de Compostela, Santiago de Compostela, 2013.
71. Gaciño, F. M.; Paredes, X.; Comuñas, M. J. P.; Fernández, J. Effect of the pressure on the viscosities of ionic liquids: Experimental values for 1-ethyl-3-methylimidazolium ethylsulfate and two bis(trifluoromethyl-sulfonyl)imide salts. *J. Chem. Thermodyn.* **2012,** 54, 302-309.

Table 1. Purity and water content of IL samples.

Ionic Liquid	Compound Name	CAS Number	Mole-fraction purity	Mass-fraction water content
$[C_2C_1Im][C_6SO_4]$	1-ethyl-3-methylimidazolium n-hexylsulfate	342573-75-5	>0.999[a]	$16 \cdot 10^{-6}$
$[P_{6,6,6,14}][(C_2F_5)_3PF_3]$	trihexyl(tetradecyl)phosphonium tris(pentafluoroethyl) trifluorophosphate	639092-18-5	0.98[b]	$11 \cdot 10^{-6}$

[a]HPLC
[b]NMR

Table 2. Viscosity values, η (mPa·s) of the ILs measured in this work[a].

	T / K					
p / MPa	298.15	313.15	323.15	333.15	343.15	353.15
	$[C_2C_1Im][C_6SO_4]$					
10.00	354	154	94.0	63.8	44.5	31.4
50.00	571	238	142	94.8	65.9	46.0
75.00	737	304	186	120	82.1	56.9
	$[P_{6,6,6,14}][(C_2F_5)_3PF_3]$					
10.00	413	189	114	78.1	53.5	37.9
50.00	913	401	223	159	112	76.3
75.00	1417	615	364	232	162	109

[a] Expanded uncertainties are $U_r(\eta) = 0.07$ for viscosity, $U(T) = 0.5$ K for temperature and $U(p) = 0.02$ MPa for pressure (k=2, level of confidence=0.95).

Table 3. Parameters of the Comuñas et al. [60] correlation for the ILs studied in this work.

	$[C_2C_1Im][C_6SO_4]$	$[P_{6,6,6,14}][(C_2F_5)_3PF_3]$
$10^2 \cdot A$/ mPa·s	9.265	3.588
B/ K	1074.7	1423.6
C/ K	166.13	142.93
D	4.125	7.971
E_0/ MPa	-828.4	684.3
E_1/ MPa·K^{-1}	5.879	-2.745
$10^3 \cdot E_2$/ MPa·K^{-2}	-6.69	5.837
AAD%	1.0	2.2

Table 4. Universal pressure-viscosity coefficient α_{film} of the ionic liquids studied in this work in GPa^{-1}

T /K	$[C_2C_1Im][C_6SO_4]$	$[P_{6,6,6,14}][(C_2F_5)_3PF_3]$
298.15	10.3	18.8
313.15	9.5	18.2
323.15	9.1	17.7
333.15	8.7	17.2
343.15	8.5	16.8
353.15	8.2	16.3

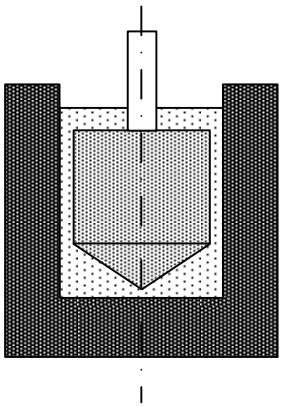

Figure 1. Coaxial cylinder system, CC25 DIN53019, used in Reologica StressTech Couette HTHP rheometer

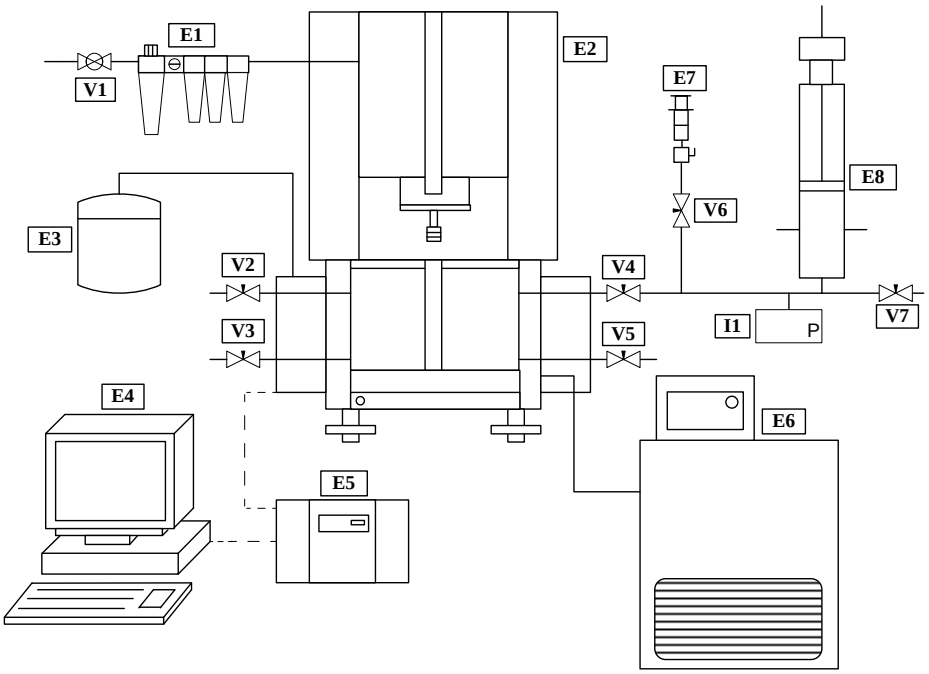

Figure 2. Schematic set-up of the high pressure rheometric technique. (E1) air filters; (E2) rheometer; (E3) motor cooler; (E4) computer; (E5) control box; (E6) thermostatic bath; (E7) glass syringe connected to Hamilton valve; (E8) piston screw pump; (V1 to V7) valves and (I1) pressure transducer.

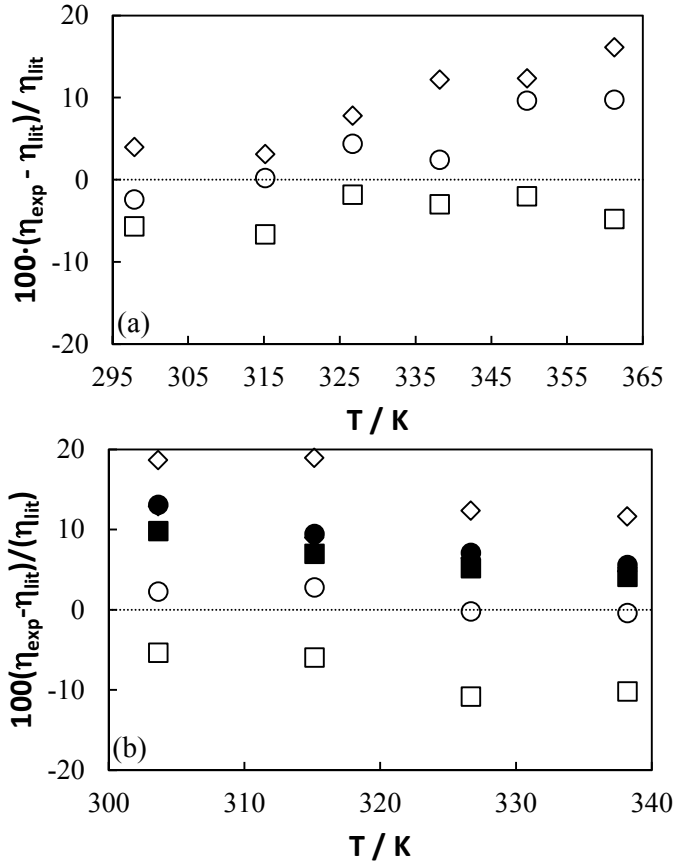

Figure 3. Relative deviations between viscosity data obtained in this work and those from Bair [58, 59] for (a) PAO40 and (b) polybutene H8 at 10MPa (□, ■), 50 MPa (○, ●) and 75 MPa (◇, ◆). Empty symbols represent comparison with reference [58] and filled symbols with reference [59].

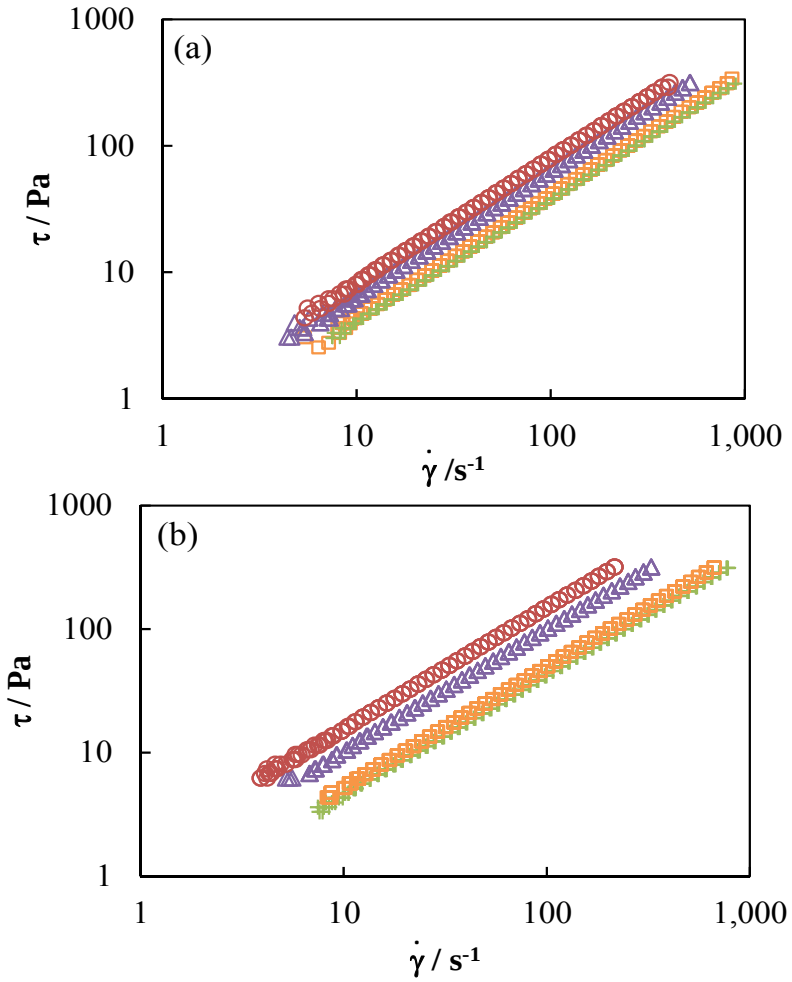

Figure 4. Flow tests at 298.15 K for (a) $[C_2C_1Im][C_6SO_4]$ and (b)$[P_{6,6,6,14}][(C_2F_5)_3PF_3]$ at 0.1 MPa (+), 10 MPa (□), 50 MPa (△) and 75 MPa (○).

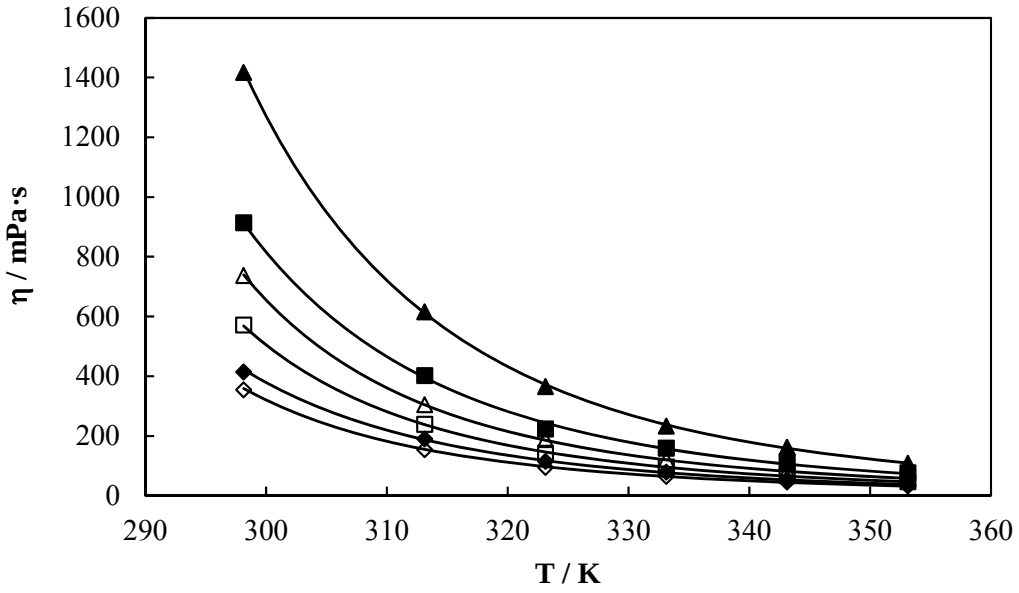

Figure 5. Viscosity values of $[C_2C_1Im][C_6SO_4]$ (empty symbols) and $[P_{6,6,6,14}][(C_2F_5)_3PF_3]$ (filled symbols) as a function of temperature for different pressures. 10 MPa (◇, ◆), 50 MPa (□, ■) and 75 MPa (△, ▲). Solid lines represent the Comuñas et al. [60] correlation (Equation 14)

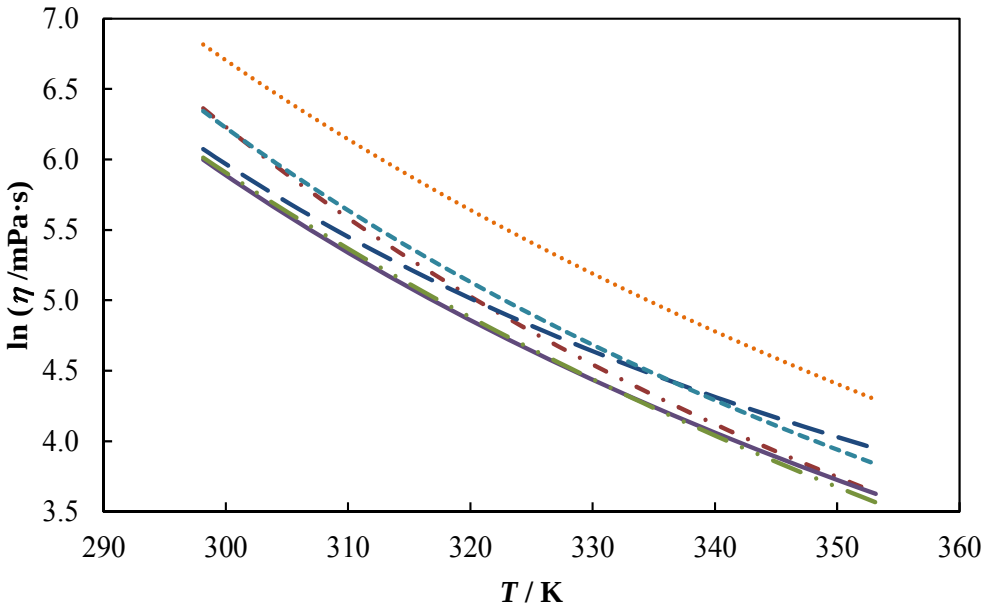

Figure 6. Viscosity values as a function of temperature at 50 MPa. $[P_{6,6,6,14}][(C_2F_5)_3PF_3]$ (dotted line), $[C_2C_1Im][C_6SO_4]$ (dashed line), mineral oil 923.M.100 [63] (dashed-dotted line), biodegradable synthetic ester 1.ES.100 [63] (solid line), polyalphaolefin 971.PAO.100 [63] (dashed-double dotted line), polyalkylene glycol 992.PG.100 [63] (long dashed line).

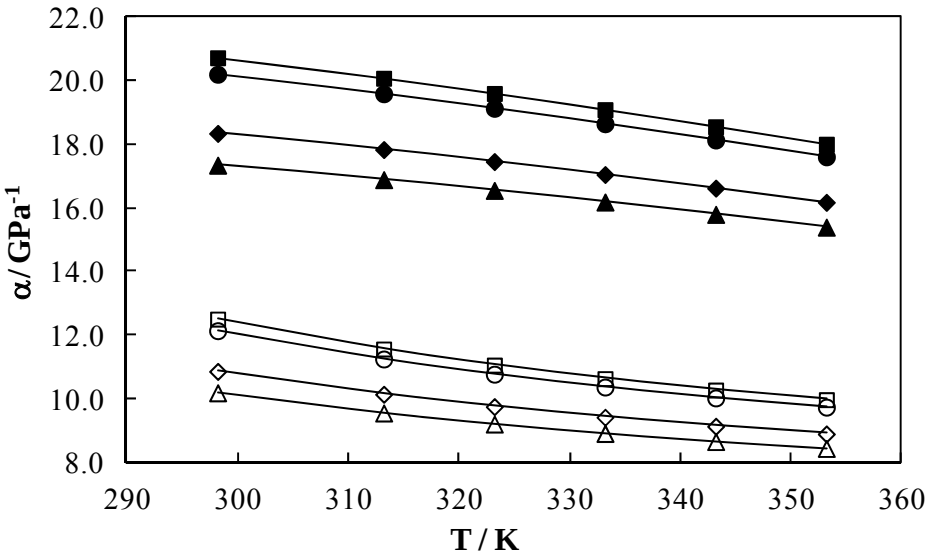

Figure 7. Local pressure-viscosity coefficient, α, of $[C_2C_1Im][C_6SO_4]$ (empty symbols) and $[P_{6,6,6,14}][(C_2F_5)_3PF_3]$ (filled symbols) as a function of temperature at 0.1 MPa (■, □), 10 MPa (●, ○), 50 MPa (◆, ◇), 75 MPa (▲, △).

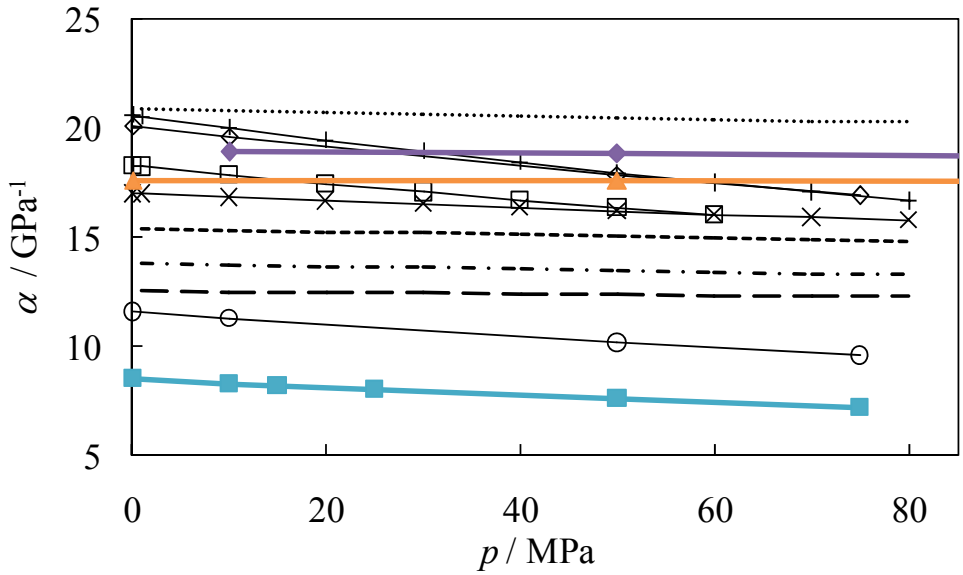

Figure 8. Local pressure-viscosity coefficient, α, at 313.15 K of mineral oil 923.M.100[63] (dotted line), squalane[40] (+), $[P_{6,6,6,14}][(C_2F_5)_3PF_3]$ (◇), $[C_4C_1Pyrr][(C_2F_5)_3PF_3]$[30] (◆), $[C_4C_1C_1Im][(C_2F_5)_3PF_3]$[61] (▲), PAG3[65] (□), $[C_1OC_2C_1Pyrr][(C_2F_5)_3PF_3]$[61] (×), polyalphaolefin 971.PAO.100[63] (dashed line), biodegradable synthetic ester 1.ES.100[63] (dashed-dotted line), polyalkyleneglycol 992.PG.100[63] (long dashed line), $[C_2C_1Im][C_6SO_4]$ (○), and $[C_2C_1Im][C_2SO_4]$[71] (■).

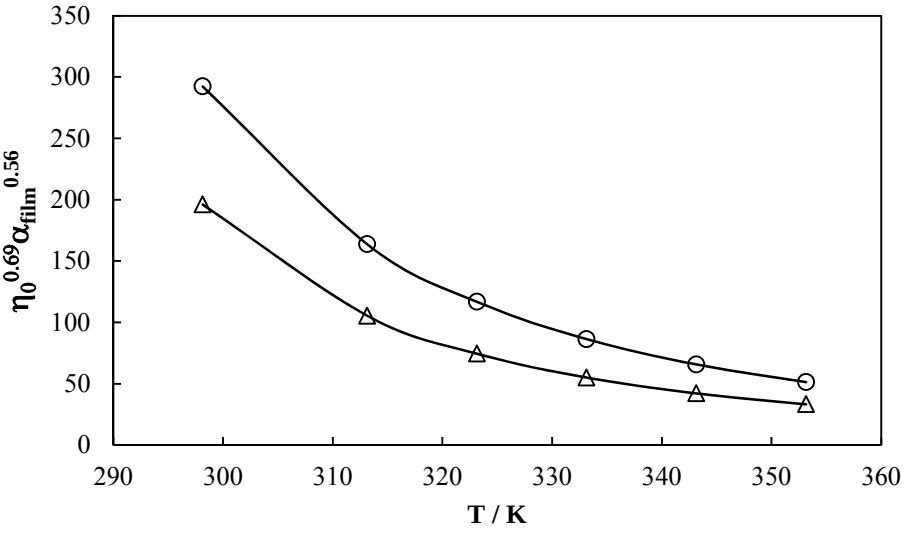

Figure 9. $\eta_0^{0.69}\alpha_{film}^{0.56}$ factor as a function of the temperature for $[C_2C_1Im][C_6SO_4]$ (△) and $[P_{6,6,6,14}][(C_2F_5)_3PF_3]$ (○).

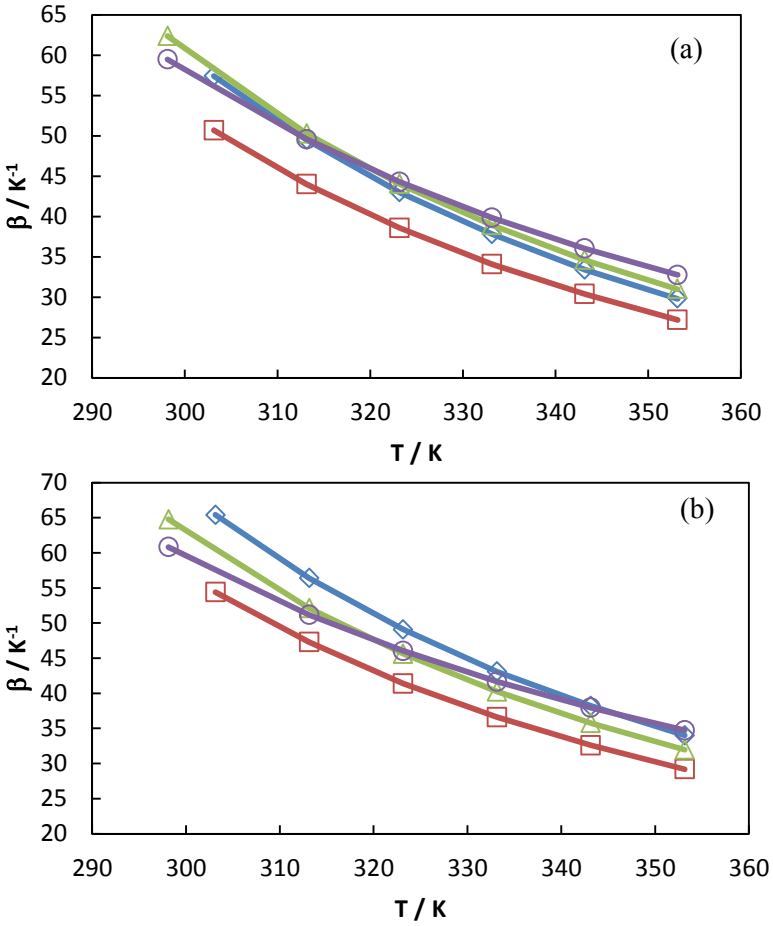

Figure 10. Local temperature-viscosity coefficient, β, of $[C_2C_1Im][C_6SO_4]$ (△), $[P_{6,6,6,14}][(C_2F_5)_3PF_3]$ (○), $[C_4C_1Pyrr][(C_2F_5)_3PF_3]$[30] (◇) and $[C_4C_1Pyrr][CF_3SO_3]$[30] (□) as a function of temperature at 10 MPa (a), and 50 MPa (b).